Characterisation of Patterned Irregularity in Locally Interacting, Spatially Extended Systems: Ventricular Fibrillation

V.N.Biktashev*

Department of Mathematical Sciences, University of Liverpool, Liverpool L69 7ZL, U.K
** on leave from: Institute for Mathematical Problems in Biology, Pushchino, Russia*

A.V.Holden

School of Biomedical Sciences, University of Leeds, Leeds LS2 9JT, U.K.

Abstract. Surface imaging of electrical activity in isolated heart tissue and computational models of ventricular fibrillation show patterned irregularity. Such irregularity in spatially extended, nonlinear systems can result from stochastic and deterministic processes. We require methods and measures for characterising these patterns, that provide insight into the mechanisms of the evolving spatio-temporal irregularity, and that can be related to simple time series measures of local or global (e.g.the electrocardiogram) activity and stochastic models.

The re-entrant ventricular arrhythmias of monomorphic ventricular tachycardia and fibrillation are produced by abnormal spatio-temporal patterns of propagation in the ventricular myocardium. These behaviours can be described by solutions of reaction-diffusion equation excitable medium models. The direct comparison of such solutions with existing experimental observations is virtually impossible as there are too many factors to be taken into account, including not only the complicated dynamics of the re-entrant waves of excitation in the tissue, but also the way the appearance of these waves on the surface is modified by the inhomogeneity, anisotropy and three-dimensional nature of heart tissue. One way of indirect comparison is to compare characteristics of the complexity of the model and the real data, that are invariant under these modifications of the signal. Karhunen-Loéve decomposition is a standard tool for evaluating the complexity of multidimensional signals. Comparison of the separate and conjoint complexities of the signals on the opposite sides of the preparation can be considered as an indicator how much three-dimensional effects are essential in the preparation behaviour.

INTRODUCTION

Many experimental irregular time series that are analysed and modeled as stochastic processes are in fact recordings obtained at a point in a spatially extended system e.g neuronal spike trains, conventionally treated as realisations of stochastic point processes [1], are in fact propagating wave trains of excitation. It is now routine to monitor activity in spatially extended systems as a sequence of images (a movie), rather than by (multiple) time series. Such image sequences are generally not periodic in space and/or time but are irregular, and this irregularity may be generated by the internal dynamics of the system, or may result from external, applied noise sources. The images may be characterised qualitatively by features, or quantitatively by measures.

The qualitative characteristics of the patterned irregularity may evolve with time. We seek to develop approaches to characterise slowly evolving patterned irregularity in systems where spatial interactions are strongly localised (by nearest neighbour interactions in spatially discretised systems), by constructing a series of computational tools that enable experimental data and numerical simulations to be visualised and quantified within the same conceptual and computational toolkit. Such spatially extensive systems with local interactions are widespread in physics, chemistry and biology; we are primarily concerned with excitable media, in which the local interaction can be represented by a diffusion term. Qualitative changes in patterned irregularity may result from slow changes in system parameters, or by switching produced by large fluctuations. Although such a computational approach, based on signal analysis, simulations, and bifurcation analysis of models

using continuation algorithms, is well developed for time series [2] it is less well developed for movie images of sampled evolving continuous fields.

Among the approaches in this direction, an important place belongs to the Karhunen-Loève (KL) decomposition, which effectively reduces spatio-temporal data to a time series of a small dimensionality. Although it is essentially a linear tool, it can capture many important features of nonlinear spatio-temporal chaos, as it has been convincingly illustrated on two models, the Kuramoto-Sivashinsky and Muller-Huse equations in [3], and on a reaction-diffusion system describing a layered semiconductor structure in [4]. KL decomposition has been successfully used for the analysis of real experimental spatiotemporal data, *e.g.* surface chemical reactions [5] or body surface magnetic field and electric potential maps of heart activity [6,7], to name just some recent examples.

We illustrate this approach by analysing movie images of electrical activity from the surfaces of an in vitro, experimental preparation of fibrillating heart muscle, and images generated by simple mathematical models of fibrillation.

VENTRICULAR FIBRILLATION

During your life your heart beats rhythmically, at about one beat per second, with the synchronous contraction of the main pumping chambers, the ventricles, ejecting blood. During fibrillation the chambers of the heart no longer contract synchronously, but quiver and writhe, and the heart does not eject blood. Unless the fibrillation self-terminates, or is terminated by a defibrillation shock, death is imminent. Ventricular fibrillation almost invariably occurs during the process of dying, and its onset underlies sudden cardiac death. It is widely believed that the mechanism of ventricular fibrillation is that it is produced by one or many re-entrant propagating waves of excitation in the ventricular wall, that excite different parts of the wall at different times, and the same part of the wall repeatedly. The mechanical beating of the heart is triggered by excitation waves of electrical activity, with one wave triggering one heartbeat during the normal, rhythmic, synchronised beating of the heart. In re-entrant arrhythmias the same wave of excitation passes repeatedly through the same piece of tissue, repeatedly re-exciting it; contraction of the ventricular wall is no longer synchronous, the ventricle writhes and squirms and no longer acts as a pulsatile pump. Propagation of excitation in the heart can be modelled as the activity of an excitable medium, by reaction-diffusion equations; in such a medium propagating waves annihilate on collision. In an isotropic, homogeneous two dimensional medium the simplest re-entrant wave is a spiral wave. A single spiral wave can rotate rigidly, around a circular core, or its tip may meander biperiodically or erratically. The spatio-temporal disorder of electrical activity during ventricular fibrillation results from interacting propagating waves from a small fluctuating number of multiple, moving re-entrant wave sources, where the wave sources are being born at broken wavefronts and die by destructive interactions between wave sources or with the boundaries of the tissue.

Among recent successful approaches to this kind of problems is the series of papers by Rogers et al [8–11] which develop the idea that since fibrillation is made of propagating excitation waves, its analysis can be based on detecting the excitation front segments, and evaluating the statistics of their number and kinematic properties. Although this has been proved very successful, as for all essentially nonlinear methods, it inherently depends on a large amount of data of a very good quality, — otherwise, the detection of the fronts becomes problematic.

KL decomposition, being a linear tool, is significantly more robust with respect to experimental noise and lack of data. It was also successfully used for the analysis of fibrillation. Bayly et al. [12] used it to show significant increase of complexity, measured as the number of the significant KL modes at the onset of fibrillation, and then gradual decrease of that complexity during first minute of fibrillation. KenKnight et al. [13] have used KL decomposition to quantitatively describe local capture of VF by pacing. Bayly et al. [14] have used the observed behaviour of the five most significant KL modes to make short-term predictions of VF.

The purpose of the present study is to develop a tool characterising spatiotemporal complexity, which would take into account and effectively exploit the available simultaneous optical recording from opposite sides of the myocardium. This would help to give a qualitative answer to the question, to what extent is the myocardial wall three-dimensional, and in what situations should this three-dimensionality be neglected or taken into account. The KL method was chosen because of its linearity, which promises robustness, and its already proven ability not only in the formal characterisation of spatiotemporal complexity, but also to detect very specific features of fibrillation.

An excellent recent review of various methods of quantifying spatiotemporal chaos of fibrillating cardiac muscle can be found in [15]. Mechanisms for the initiation and maintenance of ventricular fibrillation are reviewed in [16], and the relations between nonlinear wave processes in excitable media and fibrillation are discussed in the Focus issue of Chaos [17] and in [18].

EXCITABLE MEDIA MODELS

Mathematical models of cardiac excitability based on voltage clamp experiments use many variables to describe each cell, and can take into account the bidomain (current flow in extra- and intracellular domains) and anisotropic nature of the cell-to-cell conductivity and tissue inhomogeneity:

$$\begin{aligned} &\partial_t E = F(E, g_j, \vec{r}) + \hat{\mathcal{D}} \cdot E, \\ &\partial_t g_i = G_i(E, g_j, \vec{r}), \\ &i, j = 1, \ldots, N, \end{aligned} \tag{1}$$

where $\vec{r}$ is a vector of spatial coordinates; E is the transmembrane voltage; $\hat{\mathcal{D}}$ is the conductivity operator, which may explicitly depend on $\vec{r}$ and is integro-differential

to take into account the bidomain structure of the tissue or degenerates into a Laplacian if it does not; and $g = (g_1, g_2 \ldots)^{\mathrm{T}}$ is a column-vector of local variables, including gating variables and ionic concentrations. In the case of biophysically detailed models of ventricular tissue [19] the excitation equations are stiff and of high order. For a monodomain, two-dimensional model of normal ventricular tissue the spiral wave solution is stable and meanders biperiodically [20,21]. Spiral wave solutions of some biophysical cardiac excitation equations are unstable [19], and break down into spatio-temporal irregularity. Such spontaneous breakdown of re-entrant activity has been proposed as a mechanism for the development of fibrillation from simple re-entry; the stability of the spiral wave solutions for normal ventricular tissue is consistent with the persistence of re-entrant ventricular tachycardia, in which the ventricles flutter at a rate ten times faster than the resting heartbeat, and suggests that breakdown into fibrillation may result from geometric effects *e.g.* rotational anisotropy.

A second-order differential operator for conductivity [22,23]:

$$\hat{\mathcal{D}} \cdot E = \sum_{i,j=1}^{3} \frac{\partial}{\partial r_i} D_{i,j}(\vec{r}) \frac{\partial E}{\partial r_j} \tag{2}$$

takes into account the rotational anisotropy of the real ventricular tissue: the direction of the fibres is the direction of the largest eigenvector of the conductivity tensor $D_{i,j}$. This direction rotates through about 120 degrees on moving from the outside (epicardial) to the inside (endocardial) surface of the ventricular wall. For a medium with simplified FitzHugh-Nagumo local kinetics, with parameters that have stable scroll waves in a homogeneous, isotropic medium, such rotational anisotropy of the tissue can be sufficient to make a simple re-entrant, transmural scroll wave unstable and lead to spatio-temporal irregularity [23].

Complicated local kinetics and complicated description of conductivity make modelling computationally expensive. Some qualitative results can be obtained for simpler models, which caricature the excitation and propagation properties of cardiac tissue. Complicated and stiff local kinetics, or inhomogeneity, or anisotropy are not required to produce complicated spatio-temporal behaviour of the excitable medium. We used for simulations the simple homogeneous FitzHugh-Nagumo ($N = 1$) excitable medium model with simple diffusion-like conductivity. At some parameter values, the scroll wave filaments in this model have negative tension, which leads to their breakup and development of a three-dimensional "turbulence" of excitation waves, resembling fibrillation [24,25].

Figure 1 near here

Figure 1 shows snapshots of spatio-temporal irregularity in this model. The surface patterns of this "numerical fibrillation" demonstrate the same qualitative features as the patterns observed in optical mapping experiments. We used for simulations the FitzHugh-Nagumo system of equations:

$$\partial_t E = \epsilon^{-1}(E - E^3/3 - g) + \nabla^2 E,$$
$$\partial_t g = \epsilon(E + \gamma - \beta g), \tag{3}$$

where $\epsilon = 0.3$, $\beta = 0.75$ and $\gamma = 0.5$, with forward-time Euler differencing with time step 0.03 t.u. (time units) and simplest seven-point approximation of the Laplacian on a rectangular grid with space step 0.5 s.u. (space units), in media of different size with non-flux boundary conditions. This choice of parameters provides negative tension of the filaments, *i.e.* scroll waves in sufficiently large media are unstable, their filaments tend to lengthen, curve, touch the boundaries and each other and break onto pieces, each of which then grows again etc. The same set of equations in two spatial dimensions shows stable spiral waves with a period of 20 t.u.. This is in qualitative correspondence with the fact that well developed fibrillation is much more common in sufficiently thick hearts or heart preparations.

SURFACE ACTIVITY

The electrical activity at a number of points on the inside or outside surfaces of the heart can be recorded during experimentally induced fibrillation, as mutiple time series with a high temporal resolution. The spatio-temporal pattern of activation can be reconstructed and viewed as a map or displayed dynamically; methods of analysing such displays of cardiac are reviewed in [15], and are based on specific features (phase maps, propagation velocity vectors, space-time plots and wavefront statistics and dynamics) or statistical measures (spatial correlation and coherence, signal decomposition as in Fourier anlaysis or Karhunen-Loéve decomposition). A higher spatial resolution can be achieved by optical monitoring of the surface electrical activity. The data we used in this study (provided by A.M.Pertsov and co-authors, SUNY Health Centre in Syracuse, USA), were from the endo- and epicardial surfaces of pieces of sheep ventricular wall, stained with a voltage-sensitive dye. The video images were obtained at a spatial resolution of 0.6 mm and temporal resolution of 8 ms. The points where the signal was too low were excluded from consideration, so the shape of the patterns represents not the excitable ventricular preparation, but merely the perfused and stained part of it, typically of the size of about $3 \times 3\,\mathrm{cm}^2$. More technical details can be found in [26,27].

Irregular, self-sustained re-entrant propagation can be induced in a resting tissue preparation by rapid electric pacing; this provides an experimental model for the electrical activity during ventricular tachycardia (high — up to about 10 Hz— frequency activity, believed to be due to simple re-entry in the ventricle) and fibrillation (irregular, high frequency activity due to multiple re-entrant sources). Figure 2 shows typical simultaneous images of endocardial and epicardial activity.

Figure 2 near here

Periods of excitation were up to about 200 ms in "monomorphic tachycardia" and in the range of 100–150 ms in "fibrillation". So we may scale the time unit of (3) roughly as 5–10 ms.

DOMAIN STRUCTURE

An important insight in understanding of the mechanism of the fibrillation, at least in the experimental data considered in this paper, has been recently achieved by Zaitsev et al. [28], who have analysed the optical recordings of electrical activity at all points of the preparation as approximately periodic processes, found their dominant frequencies, and then drawn the maps of the distribution of dominant frequencies over the preparation. This has revealed something totally unexpected, a domain structure of the dominant frequencies, with almost the same dominant frequencies within one domain and sharp interfaces between the domains. The detection of a single dominant frequency is, of course, a strongly nonlinear procedure. In this section we illustrate how this domain structure looks when analysed using linear filtering.

We performed discrete Fourier transform on both the simulation and tissue experimental data $u(x, y, t)$,

$$\tilde{u}(x, y, f) = \mathcal{F}[u(x, y, t)] \tag{4}$$

to obtain power spectra,

$$P(f) = \int \int |\tilde{u}(x, y, f)|^2 dx dy, \tag{5}$$

which were analysed visually to find the location and width of two or three main frequency peaks [29,30].

Figure 3 near here

Figure 3 shows typical experimental frequency domains. Panels (a)–(c) show the spatial distribution of the oscillation power over the preparation, with the low frequency component in (a) and the high frequency in (c). The power spectra of the whole preparation (solid line), and the bandpass filters used to extract the three principal frequencies are shown on panel (d). The feature of the total power spectrum is that different frequencies of oscillations are spatially separated, in three domains. This is visually confirmed by the time series recorded at points in different domains, panel (e).

In this case, we have found three main frequency peaks with frequency ratio approximately $2 : 3 : 4$, and three spatially distinct frequency domains. There are clear borders between the different domains. Figure 4 shows Lissajous figures of

three points chosen in three different domains. In this case, the synchronous character of these signals is evident. The simplest interpretation for the behaviour seen in this particular experiment is there was only one re-entrant source, with frequency of 9.6 Hz (close to that of spiral wave solutions of biophysical models of ventricular tissue) , and this frequency was divided in the ratio $2:3$ and $1:2$ in different parts of the preparation. In cardiology, such frequency division by simple ratios is produced by alternating propagation failure, due to a spatial inhomogeneity, and is called Wenckebach frequency division.

Figure 4 near here

In [29,30] we used this method of the analysis of the spatiotemporal data to compare two alternative hypotheses for the mechanism of the domain structure of the fibrillation. We have identified diagnostic features potentially important for discriminating between the two hypotheses. Some of these features, such as the domains overlap coefficient, only makes sense in terms of the linear analysis and is completely lost after detecting a single dominant frequency for each point.

KARHUNEN-LOEVE DECOMPOSITION

Karhunen-Loeve (KL) decomposition is an eigenvalue decomposition of the autocorrelation matrix (spatial autocorrelation function) of the signal. If we consider the concatenation of the two concurrently recorded endo- and epicardial surface signals, by analysing KL spectra and empirical eigenvectors obtained for the conjoint signal and for its components separately, we are able to diagnose two extreme situations: the two signals being completely linearly dependent, or completely linearly independent.

Let signal $z(t)$, $z \in \mathbb{R}^{2n}$, $t \in [0,T]$, be concatenation of two subsignals,

$$z(t) = \begin{pmatrix} x(t) \\ y(t) \end{pmatrix}, \quad x \in \mathbb{R}^n, \quad y \in \mathbb{R}^n \tag{6}$$

For our present application, x and y are the records from the opposite surfaces, and n is the number of pixels on each of the surfaces. We consider these numbers identical for both signals, just for the sake of brevity.

KL decomposition is eigenvalue decomposition of the autocorrelation matrix (aka spatial autocorrelation function) of the signal, which for signal z is [31]

$$\overline{zz^+} = \frac{1}{T}\int_0^T z(t)z^+(t)\,\mathrm{d}t. \tag{7}$$

Here and below, the $+$ superscript denotes matrix transposition. Substituting (6) into this definition gives

$$\overline{zz^+} = \begin{pmatrix} \overline{xx^+} & \overline{xy^+} \\ \overline{yx^+} & \overline{yy^+} \end{pmatrix}, \tag{8}$$

the autocorrelation matrix of the composite signal has a block structure. The diagonal blocks of this matrix are the autocorrelation matrices of each of the components x and y, and off-diagonal blocks are the cross-correlation matrix between the two signals and its transpose.

There are two interesting cases:

1. Statistically independent signals. Suppose the cross-correlation function $\overline{xy^+}$ vanishes, then $\overline{zz^+} = \overline{xx^+} \oplus \overline{yy^+}$ and the eigenvalue problem for the correlation matrix of z

$$\overline{zz^+} Z_j = \lambda_j Z_j \tag{9}$$

is reduced to that of the eigenvalue problems of the components' correlation matrices,

$$\overline{xx^+} X_k = \mu_k X_k \quad \text{and} \quad \overline{yy^+} Y_l = \nu_l Y_l. \tag{10}$$

Thus,

$$Z_j = \begin{pmatrix} X_k \\ 0 \end{pmatrix} \text{ or } \begin{pmatrix} 0 \\ Y_l \end{pmatrix}, \quad \{\lambda_j\} = \{\mu_k\} \cup \{\nu_l\}. \tag{11}$$

Strictly speaking, Z_j might have both components nonzero only in the unlikely event that some of μ_k exactly coincide with some of ν_l.

2. Linearly dependent signals. Suppose both subsignals x and y can be obtained by two different linear transformations of the same low-dimensional "hidden" signal u,

$$x(t) = \Xi u(t), \quad y(t) = \mathrm{H} u(t), \tag{12}$$

where $u \in \mathbb{R}^m$, and m may be different from n, say $m < n$, and Ξ and H are constant matrices of the format $m \times n$. More specifically, we assume that the matrices obey the conditions:

$$\Xi^+ \Xi = \xi \mathrm{I}, \quad \mathrm{H}^+ \mathrm{H} = \eta \mathrm{I}, \tag{13}$$

where I is the identity matrix. These conditions might appear too restrictive, but (a) for $m = 1$ they are always true, and (b) for $m \geq 2$ some restrictions are necessary, otherwise if say x depends only on on the first component of u and y depends only on the second component of u, they need not be in any way dependent.

Let U_p be the eigenvectors and σ_p corresponding eigenvalues of the hidden signal,

$$\overline{uu^+}U_p = \sigma_p U_p. \tag{14}$$

Then

$$\overline{zz^+}\begin{pmatrix} \Xi \\ \mathrm{H} \end{pmatrix} U_p = \begin{pmatrix} \Xi \\ \mathrm{H} \end{pmatrix} \overline{uu^+}\left(\Xi^+, \mathrm{H}^+\right) \begin{pmatrix} \Xi \\ \mathrm{H} \end{pmatrix} U_p$$

$$= \begin{pmatrix} \Xi \\ \mathrm{H} \end{pmatrix} \overline{uu^+}\left(\Xi^+\Xi + \mathrm{H}^+\mathrm{H}\right) U_p = (\xi+\eta) \begin{pmatrix} \Xi \\ \mathrm{H} \end{pmatrix} \overline{uu^+}U_p = (\xi+\eta)\sigma_p \begin{pmatrix} \Xi \\ \mathrm{H} \end{pmatrix} U_p,$$

that is, z-eigenvectors are images of u-eigenvectors,

$$Z_j = \begin{pmatrix} \Xi \\ \mathrm{H} \end{pmatrix} U_p, \tag{15}$$

and z-eigenvalues are proportional to u-eigenvalues,

$$\lambda_j = (\xi + \eta)\sigma_j. \tag{16}$$

Similarly,

$$X_j = \Xi U_j, \quad \mu_j = \xi\sigma_j, \quad Y_j = \mathrm{H}U_j, \quad \nu_j = \eta\sigma_j. \tag{17}$$

Excluding now the hidden signal from consideration, we see that

$$Z_j = \begin{pmatrix} X_j \\ Y_j \end{pmatrix}, \quad \mu_j = \alpha\lambda_j, \quad \nu_j = \beta\lambda_j, \quad \text{where} \quad \alpha + \beta = 1. \tag{18}$$

To summarise, by analysing KL spectra and empirical eigenvectors obtained for the composed signal and for its components separately, we are able to diagnose two extreme situations. If

- the joint eigenvectors have one component prevailing over the other,
- prevailing components are close to corresponding empirical eigenvectors of the subsignals, and
- each eigenvalue of the signal is approximately equal to an eigenvalue of either subsignal, and each subsignal eigenvalue corresponding only to one joint eigenvalue,

then we have (11) approximately fulfilled, which means that the signals are statistically independent. If, on the contrary

- both components of each of the joint eigenvectors are close, up to a constant factor and sign, to corresponding eigenvectors of the subsignals,

- eigenvectors of the subsignals are approximately proportional to each other, and
- eigenvectors of the joint signal are sums of the corresponding eigenvectors of the subsignals,

then (18) is fulfilled, and there is strong linear dependence between the subsignals, *i.e.* they are consequences of the same low-dimensional signal.

DIFFERENT ASPECTS OF COMPLEXITY

The complexity of the experimental and model patterns can be characterised in different ways:

- Apparent complexity of the patterns on the surface, or individual recordings,
- Behavioural complexity, as the number of "independent causes" that could produce the observed signals,

The first type of complexity may use either spatial distribution or temporal dependence of a signal separately; the second type requires joint analysis of the spatial and temporal behaviour.

The analysis of the dominant frequency distribution and its domain structure uses both temporal behaviour of individual point recordings, to establish the point spectra, and then the spatial behaviour of this spectra; yet it only gives the apparent complexity, and further conjoint analysis of the mutual behaviour of signals at different points, as by Lissajous figures, can reveal the underlying behavioural complexity, i.e. single vs multiple re-entry sources.

The KL analysis uses both temporal and spatial characteristics of the signals in the same procedure, thus it is potentially more capable of revealing the inherent behavioural complexity, such as number of individual re-entry sources or their specific features. One approach using KL analysis and focusing attention on the three-dimensional aspects, is the comparison of the conjoint and separate KL eigendata for opposite surfaces of the tissue.

We illustrate this first for two clear-cut examples, on Figures 5–7 and Figures 8–10.

Figure 5 near here

Figure 6 near here

Figure 7 near here

Figure 5 shows a stable re-entry inside a medium, which generates periodic patterns on both sides with stable period. Correspondingly, the sum of KL spectra of

separate sides approximately coincides with the KL spectrum of the concatenated (conjoint) signal, see Figure 6, where there is only a 20% difference between the leading eigenvalue for the sum of the separate spectra and the conjoint spectrum. The behaviour of the KL modes shown on Figure 7 also confirms that the corresponding separate and conjoint modes approximately coincide with each other. This clearly corresponds to the case of linear dependence of the signals as described above.

Figure 8 near here

Figure 9 near here

Figure 10 near here

Figure 8 illustrates the opposite case. Here there is a double scroll wave in the medium, which behaves in an unstable way, so the filaments of the two re-entry vortices constantly change their shape and meander. Thus the surface excitation patterns, although having roughly the same apparent complexity, have a much less stable period, and are much less independent on each other, as each of the re-entry vortices change its position in the medium significantly between the moments when its excitation wave arrives at one or the other surface. Thus the KL spectra, Figure 9, show a significant difference compared to Figure 6: the sum of separate spectra is in no sense close to the conjoint spectrum; e.g. the conjoint leading eigenvalue is more than 60% higher than the sum of leading separate eigenvalues, and the conjoint spectrum decays manifestly slower. This is also confirmed by the visual analysis of the KL modes, Figure 10: the separate eigenmodes coincide, up to the sign, to the components of the conjoint eigenmodes, but each conjoint eigenmode has only one of the components effectively nonzero, the other being much less. This clearly corresponds to the statistical independence of the signals, as described above.

Note that in both cases, the apparent complexity was comparable, and the difference in the behaviour was influenced by stable position of the re-entry filament in one case as opposed to violent meander of the filaments in the other case.

Figure 11 near here

Figure 12 near here

A more complicated case is illustrated by Figures 11 and 12, which present the KL analysis of the the modelled data from the simulation that generated Figure 1. The conjoint KL spectrum of the concatenated signal of the two surfaces is close to the sum of the component spectra, but there is no clear domination of one surface over the other in the conjoint modes, and the resemblance of components

of the conjoint modes with separate modes is only limited. Thus, here we have an intermediate situation, where the activities on the opposite surfaces are partly correlated with each other, and partly are caused by independent events. This is despite the fact that the overall apparent complexity of this regime is clearly higher than that of the meandering double scroll of Figure 8, as here we have many (6, in the time average) filaments describing complicated movements. An explanation of this paradox is that when a filament joins the two opposite surfaces then the activities it induces on these surfaces are correlated with each other; if it does not, then the activities on opposite surfaces are generated by excitation waves sent by the filament at different moments into different directions, thus the correlation is weak if the filament is moving.

Having considered the model situation with answer known, we can now apply this technique to the experimental data.

Figure 13 presents a monomorphic tachycardia with a simple excitation patterns, and Figure 14 shows the results of KL analysis. Only two KL modes are significant, the conjoint KL spectrum is very close to the sum of the separate KL spectra, and the conjoint modes are very similar to the separate modes. Thus both epi- and endocardial sequences are probably produced by one and the same stable re-entrant source inside the medium, — a conclusion which is in a perfect agreement with the visual analysis.

Figure 13 near here

Figure 14 near here

Figure 15 illustrates a later, polymorphic stage of the tachycardia in the same experimental preparation. Its KL analysis is shown on Figures 16 and 17. Here the situation is more complicated and qualitatively resembles that of the scroll turbulence of Figures 1, 11 and 12. Thus these surface patterns are probably produced by a common source *i.e.* are two-dimensional surface views of a simple three-dimensional structure within the ventricular wall, however, the influence of this common source is modulated by factors different for these two surfaces, which may be medium inhomogeneities inducing a Wenckebach rhythm modifications or transmural movements of the re-entry block.

Figure 15 near here

Figure 16 near here

Figure 17 near here

The next two figures, 18 and 19 show the KL analysis for the experimental data illustrated on Figure 2. Here the situation is similar to the previous, i.e. partial

correlation between the two surfaces. This kind of relationship is the rule for the polymorphic tachycardia from the described experimental model.

Figure 18 near here

Figure 19 near here

It is interesting to compare the results of the KL analysis and frequency domain structure in the same preparation, see Figure 20. It would be reasonable to expect that, if the frequency domains indeed represent clusters of data that oscillate more or less coherently, but oscillations of different domains are with poorly commensurate frequencies, and thus statistically independent, then the KL decomposition should detect the presence of these coherent and independent structures, and we should see them as the principal KL modes. In reality, the coherence within the domains is not ideal and the frequencies are not quite independent, so the ideal picture is not attained; still, a strong resemblance between the shape of the frequency domains and some of the main KL modes can be seen.

Figure 20 near here

The above analysis of the KL spectra and modes is qualitative. These data can also be used for a quantitative characterisation of the complexity, e.g. via the spectral entropy defined as

$$S = -\sum_j p_j \log p_j, \qquad \text{where} \qquad p_j = \frac{\lambda_j}{\sum\limits_j \lambda_j}, \tag{19}$$

and λ_j are the KL eigenvalues. The spectral entropies of the numerical and experimental sequences considered above are summarised in Table 1.

Figure	Top/lft/epi	Bot/rgt/endo	Conjoint
Stable twisted scroll Figure 5	1.01	1.04	1.43
Meandering double scroll Figure 8	2.07	2.23	2.76
Scroll "turbulence" Figure 1	3.09	3.09	3.38
Monomorphic tachycardia Figure 13	0.22	0.72	0.64
Polymorphic tachycardia Figure 15	2.25	2.01	2.36
Polymorphic tachycardia Figure 2	2.75	2.48	3.00

TABLE 1. KL entropies of experimental and numerical datasets

As it can be easily seen, for the case of linearly dependent signals, the entropies of the components are equal to the entropy of the conjoint signal. Indeed, in this case, according to (18), $\mu_j = \alpha\lambda_j$, where α does not depend on j, thus for μ_j, the corresponding fractions $p_j = \mu_k / \sum \mu_j = \alpha\lambda_j / \sum \alpha\lambda_j = \lambda_j / \sum \lambda_j$, i.e. the same as

for λ_j. Consequently, the entropies (19) will be the same for μ_j as for λ_j; similarly for ν_j. Thus the difference between the joint entropy and those of the components is yet another indicator of the complexity of the sequence.

From Table 1, the entropies of the components of simple and double scrolls in the model (significantly correlated) differ by up to 40% from corresponding conjoint entropies, while those of scroll turbulence (fairly independent) are within 10% of each other. Similarly, the entropies of the components of the monomorphic tachycardia (strongly correlated) differ more than 3 fold, whereas those of both polymorphic tachycardias (fairly independent) are within 15% of each other. However, we believe that, as the phenomenon of fibrillation is so rich, attempts to reduce the estimation of its complexity to a single number would inevitably lead to loss of some essential features; thus the full KL spectra may have their own diagnostic value.

CONCLUSIONS AND OPEN QUESTIONS

This application of standard data processing techniques to a practical example of spatio-temporal irregularity has led to some insights into the processes of fibrillation. We have shown that the correlation of spatiotemporal activities on the opposite surfaces of the myocardium depends on the complexity of the processes in its volume, and that this dependence is consistent with the current picture of fibrillation as an ensemble of one or more scroll waves of excitation in the tissue. This was based on comparison of KL spectra of separate and conjoint signals, i.e. many parameters. Whether this can be efficiently reduced to a single numerical criterion, remains an open question. However, this has done little more than providing supporting evidence for pre-existing beliefs derived from simple visual inspection of the activity. A major function of any proposed technique will be to reduce the large amount of information in the space-time series, so a movie sequence (essentially a highly multivariate time series) is replaced by a lower, maybe univariate time series amenable to simple dynamic or stochastic modelling. The success of such approach in the study [14] together with the sensitivity of KL spectra to 3D events demostrated here, encourage further investigation of KL decomposition as a possible tool for reconstructing the three-dimensional activity based on surface observation. Another question for further study is how this interpretation of the KL modes and spectra will be modified by taking into account the domain structure, and how this would depend on the precise mechanism of this structure. The method of Lissajous figures used in [29,30] was based on point recordings and required careful filtering; it is possible that the KL analysis would make that method more informative and robust.

ACKNOWLEDGEMENTS

Authors are grateful to S.F. Mironov, A.M. Pertsov and A.V. Zaitsev for the experimental data analysed in this study, and to D.S. Broomhead for fruitful dis-

cussions and valuable suggestions. This work was supported in part by a grant from EPSRC (UK).

REFERENCES

1. A. V. Holden, *Models of the Stochastic Activity of Neurones* (Springer-Verlag, Berlin, 1976).
2. A. V. Holden, J. Hyde, M. A. Muhamad, and H. G. Zhang, in *Coupled Oscillating Neurons*, edited by J. G. Taylor and C. L. T. Mannion (Springer-Verlag, London, 1992), pp. 41–80.
3. S. M. Zoldi and H. S. Greenside, Phys. Rev. Lett. **78**, 1687 (1997).
4. M. Meixner, S. M. Zoldi, S. Bose, and E. Scholl, Phys. Rev. E **61**, 1382 (2000).
5. Y. Suchorski, J. Beben, and R. Imbihl, Surface Science **454**, 331 (2000).
6. G. Stroink *et al.*, PACE **22**, 1718 (1999).
7. R. Hren *et al.*, PACE **22**, 1292 (1999).
8. J. M. Rogers *et al.*, Ann. Biomed. Eng. **25**, 749 (1997).
9. J. M. Rogers *et al.*, Ann. Biomed. Eng. **25**, 761 (1997).
10. J. Huang *et al.*, J. Cardiovasc. Electrophysiol. **9**, 1291 (1998).
11. J. M. Rogers, J. Huang, W. M. Smith, and R. E. Ideker, Circ. Res. **84**, 945 (1999).
12. P. V. Bayly *et al.*, in *Proc Computers in Cardiology*, edited by A. Murray and R. Arzbaecher (IEEE Computer Society Press, Londong, 1993), pp. 53–56.
13. B. H. KenKnight *et al.*, in *Proc. IEEE Engineering in Medicine and Biology Society* (Institute of Electrical and Electronic Engineers, Inc., Montreal, Canada, 1995), pp. 349–350.
14. P. Bayly *et al.*, IEEE Trans. Biomed. Eng. **42**, 898 (1995).
15. J. M. Rogers, B. P. V., R. E. Ideker, and W. M. Smith, IEEE Engineering in Medicine and Biology Magazine **17**, 62 (1998).
16. J. Jalife, Ann. Rev. Physiol. **62**, 25 (2000).
17. *Ventricular Fibrillation in Normal Myocardium*, edited by A. T. Winfree (Chaos **8**, focus issue, 1998).
18. J. Jalife, R. A. Gray, and J. Chen, in *Cardiac Electrophysiology — from Cell to Bedside – 3rd edition*, edited by D. P. Zipes and J. Jalife (W. B Saunders Co, Philadelphia, 1999), pp. 386–395.
19. *Computational Biology of the Heart*, edited by A. V. Panfilov and A. V. Holden (John Wiley & Sons, Chichester, 1997).
20. V. N. Biktashev and A. V. Holden, Proc. Roy. Soc. Lond. ser. B **263**, 1373 (1996).
21. V. N. Biktashev and A. Holden, Chaos **8**, 48 (1998).
22. A. V. Panfilov and J. P. Keener, Physica D **84**, 545 (1995).
23. F. Fenton and A. Karma, Chaos **8**, 20 (1998).
24. V. N. Biktashev, A. V. Holden, and H. Zhang, Phil. Trans. Roy. Soc. Lond. ser. A **347**, 611 (1994).
25. V. N. Biktashev, Int. J. of Bifurcation and Chaos **8**, 677 (1998).
26. A. M. Pertsov *et al.*, Circ. Res. **72**, 631 (1993).
27. V. N. Biktashev *et al.*, Int. J. of Bifurcation and Chaos **9**, 694 (1999).

28. A. V. Zaitsev *et al.*, Circ. Res. **86**, 408 (2000).
29. V. N. Biktashev *et al.*, J. Physiol. **518P**, 38P (1999).
30. V. N. Biktashev *et al.*, Int. J. of Bifurcation and Chaos , to appear.
31. Note that this is spatial autocorrelation matrix, i.e. it measures correlation between spatially separated simultaneous signals — as opposed to the more often used temporal auto/cross-correlation functions, which measure correlation of a signal with itself or other signal shifted by a time delay τ.

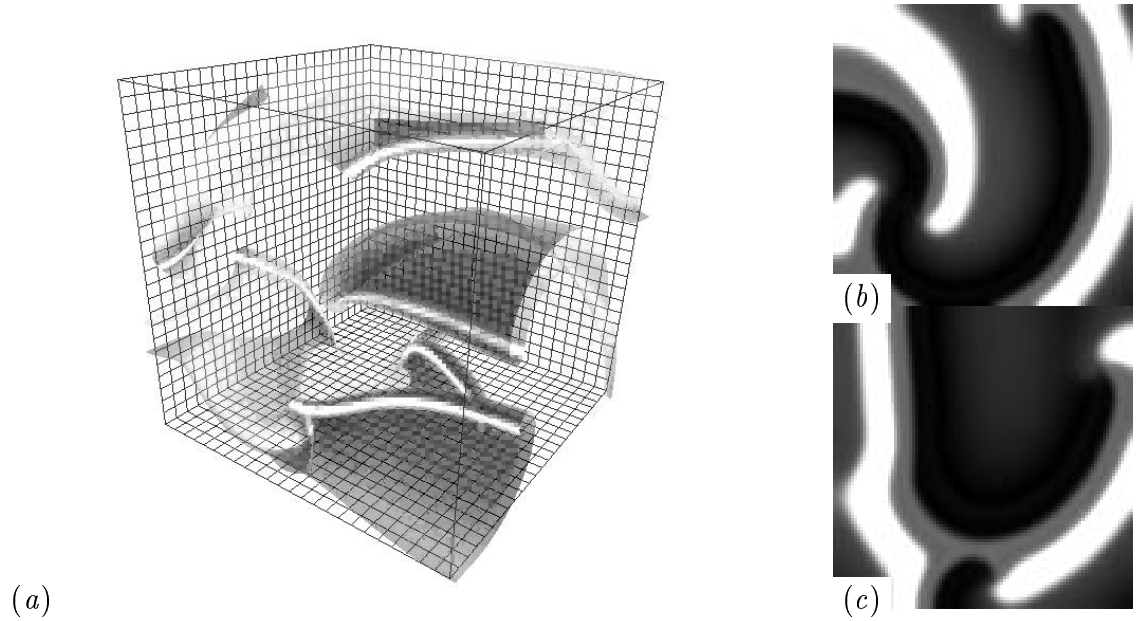

FIGURE 1. (a) Snapshot of a fibrillation-like activity in the mathematical model, medium size 50^3. The semi-transparent surfaces are the excitation wavefronts, that end in opaque curved rods, their scroll filaments. (b,c) Snapshot of activation patterns on the (b) top and (c) bottom surfaces. Excitation is shown by white.

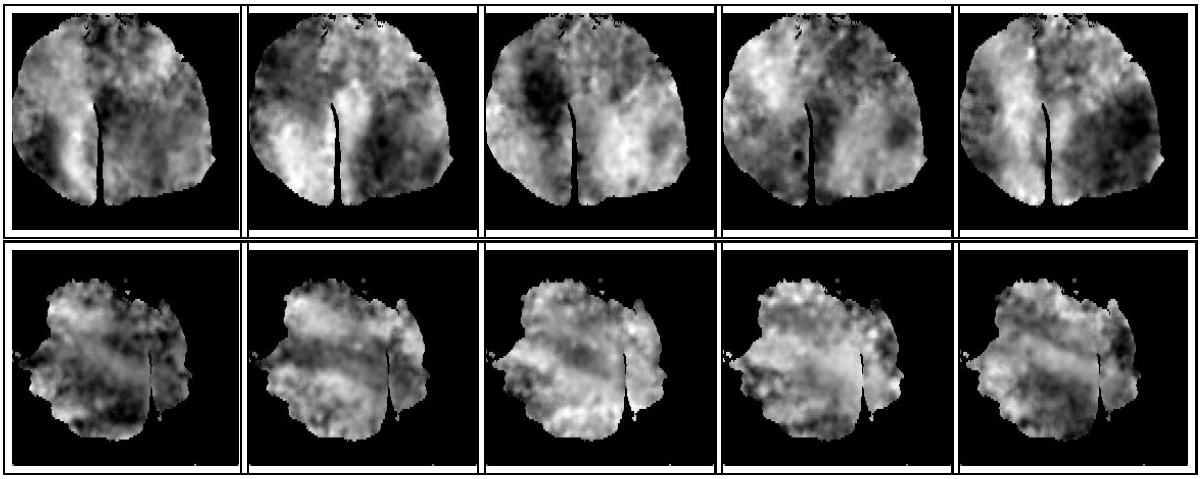

FIGURE 2. Typical experimental frames of surface electrical activity during a fibrillation episode. Upper row: epicardial view. Lower row: synchronous endocardial view. Left to right: time interval 33 ms. Excitation is shown by white.

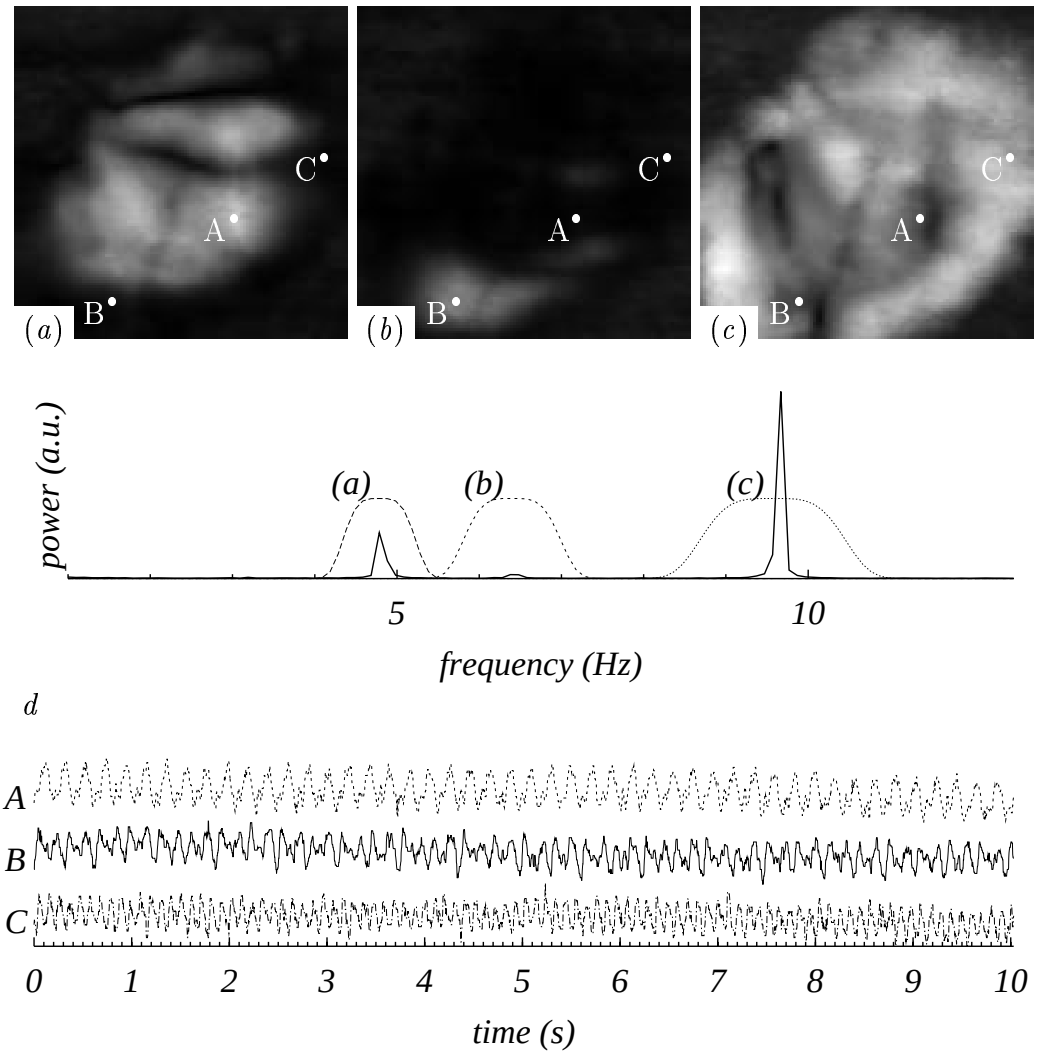

FIGURE 3. Dominant frequency domains in the experimental model of fibrillation. (a)–(c) Spatial distribution of the frequency components of the signal power (black is zero, white is the maximal value), each frame represents a square piece of surface of approximately 3 cm in size. (d) The cumulative power spectrum and the windows (dashed lines) used to extract the frequency components shown. (e) Signals recorded at points A, B and C designated on (a)–(c). It is possible that the highest frequency domain (c) is synchronous with the re-entrant source, while the two other domains correspond to Wenckebach divided frequencies with ratios 1:2 and 2:3.

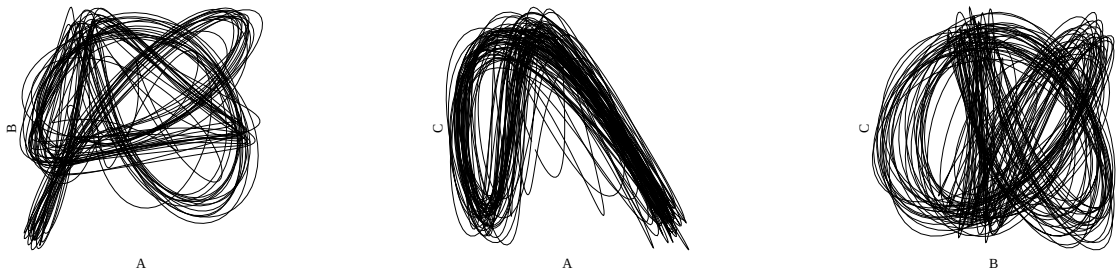

FIGURE 4. Lissajous figures of the filtered recordings from points A, B and C of Figure 3.

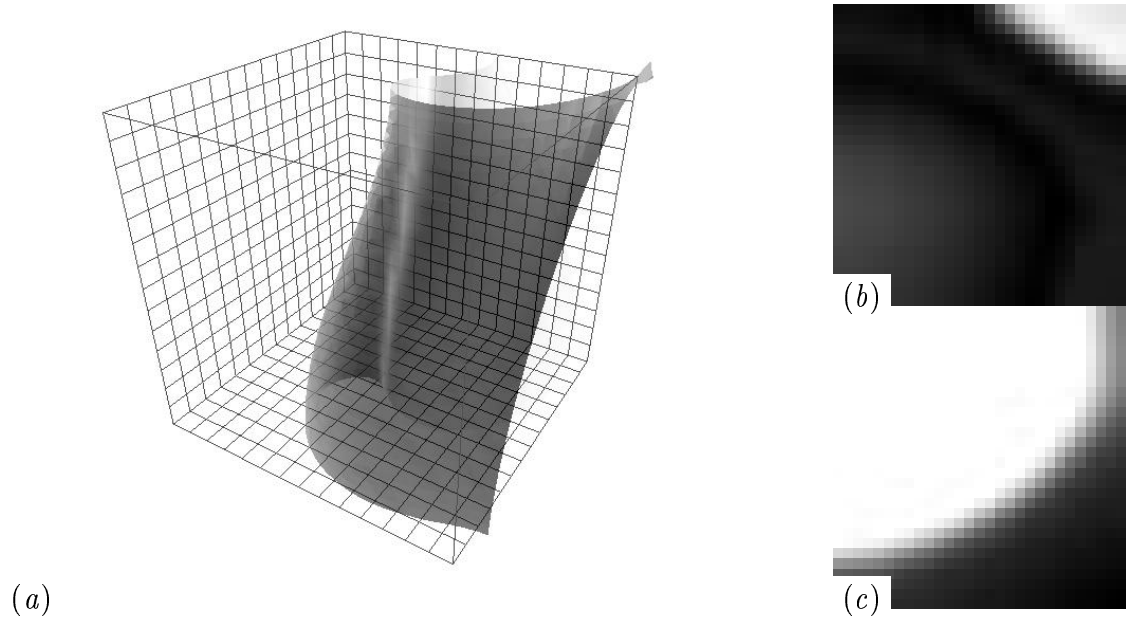

FIGURE 5. A twisted scroll wave with a stable period, medium size 15^3, parameters as described in text except β has a gradient along the z-axis from 0.646 to 0.714. Notations the same as in Figure 1.

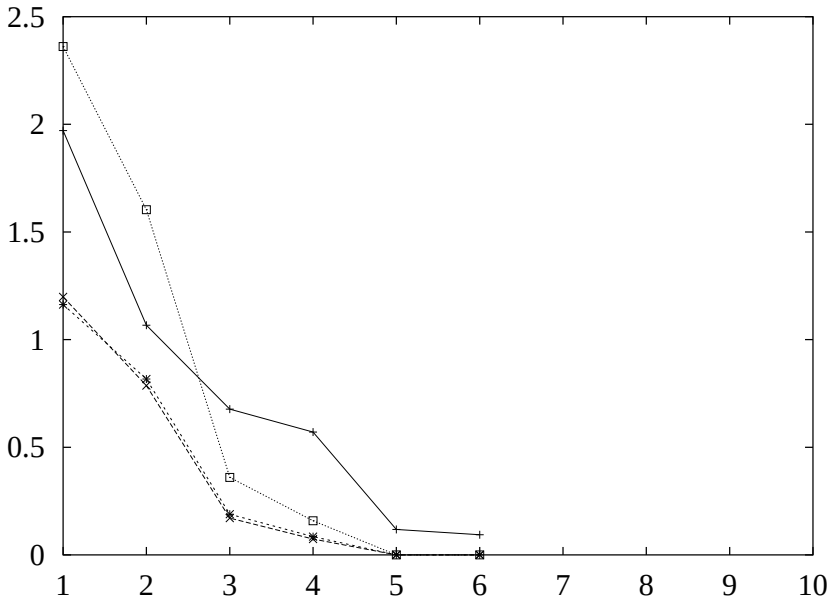

FIGURE 6. KL spectra of the surface patterns in the numerical simulations of of the stable twisted scroll shown on Figure 5: amplitudes of eigenfunctions vs their ordinal number. "+": spectrum of both surfaces processed together; "×" and "∗": spectra of the two surfaces processed separately; "□": sum of the two separate spectra.

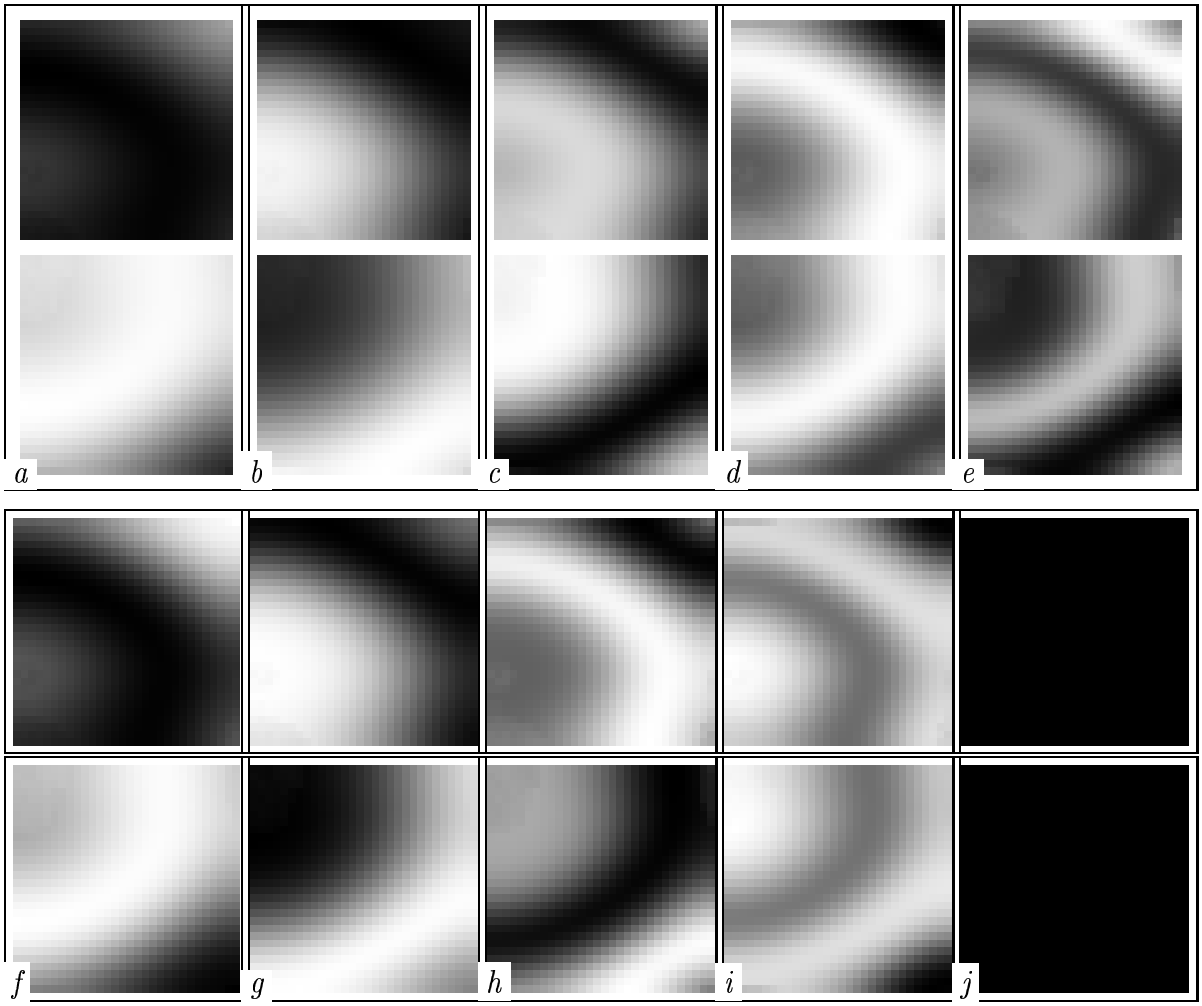

FIGURE 7. The principal KL modes of the surface patterns from the numeric stable twisted scroll of Figure 5, (*a*–*e*) processed together, (*a*) most powerful mode, (*e*) fifth most powerful mode, (*f*–*j*) processed separately, (*a*) most powerful mode, (*e*) fifth most powerful mode. Top rows: top surface, bottom rows: bottom surface.

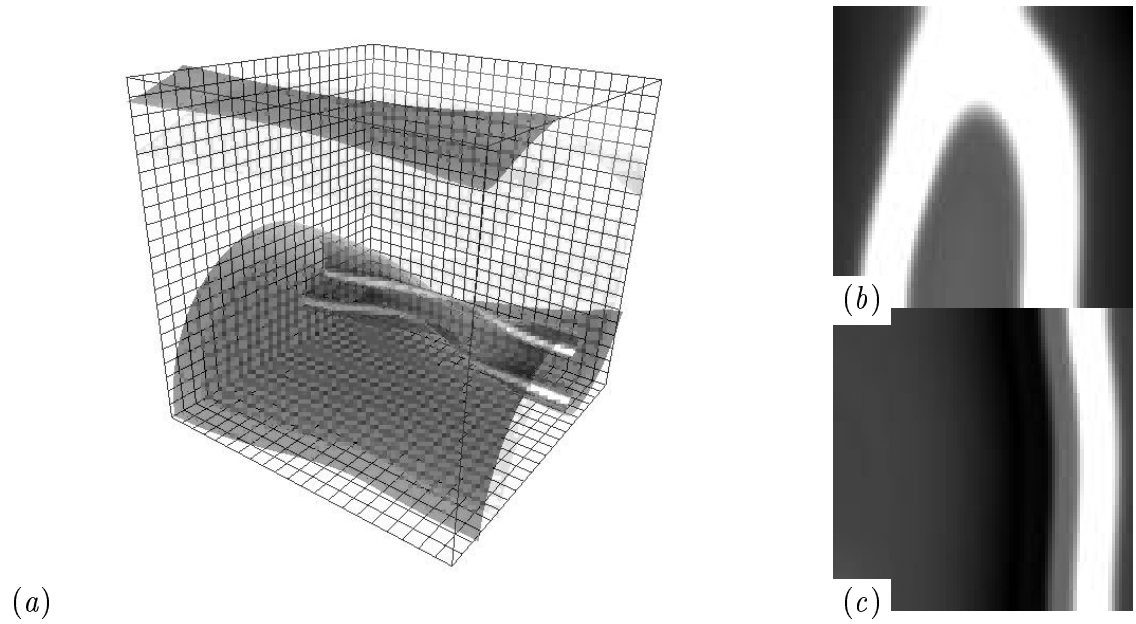

FIGURE 8. Meandering double scroll wave, medium size 43^3. Notations the same as in Figure 1.

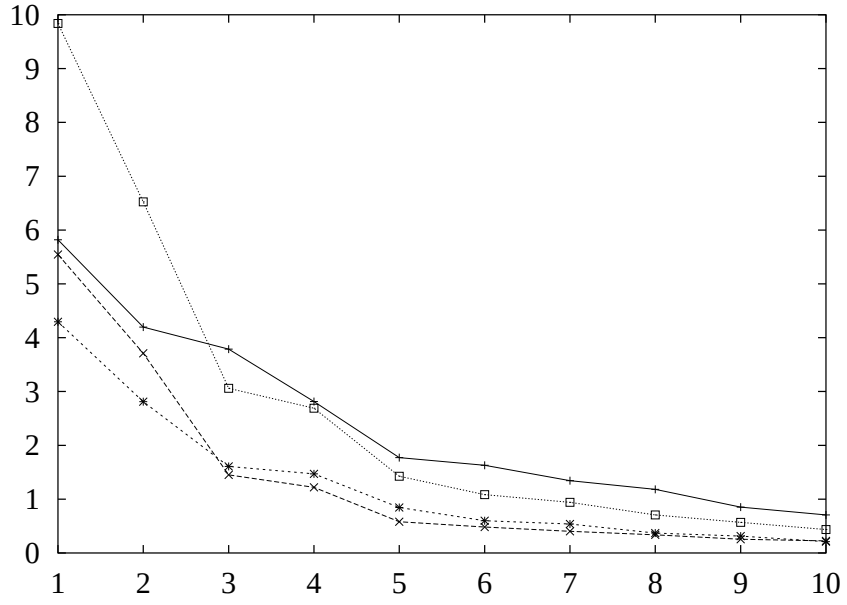

FIGURE 9. KL spectra of the surface patterns of the numerical meandering double scroll Figure 8, same format as in Figure 6. Note that the joint spectrum ("+") is significantly different from the sum of separate spectra ("□").

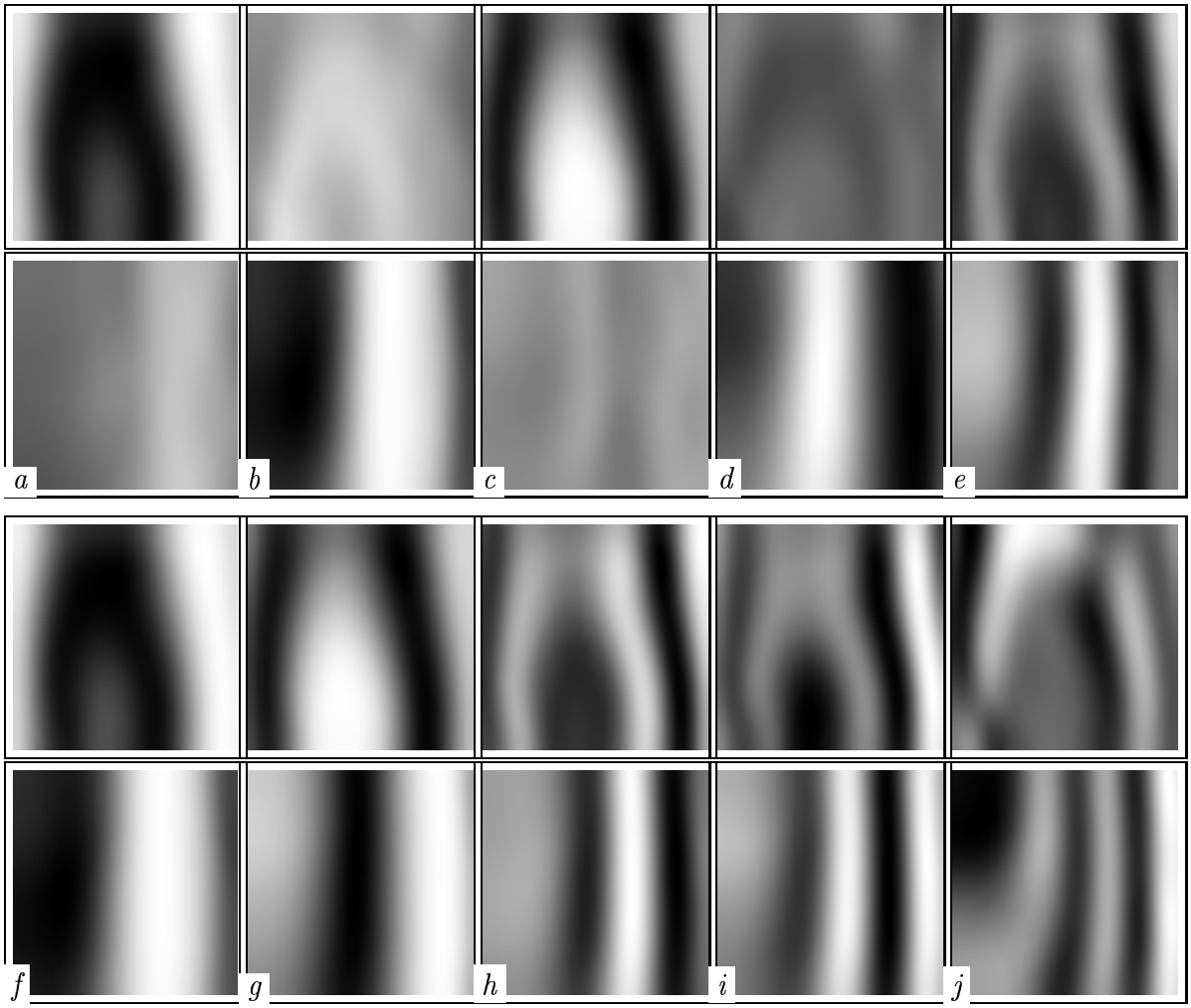

FIGURE 10. The principal 3 KL modes of the surface patterns from the numerical meandering double scroll Figure 8. Same format as in Figure 7. Note that for most principal modes, the amplitude of one side (top(a), bottom(b), top(c), bottom(d)) is much larger than on the other side (bottom(a), top(b), bottom(c), top(d)). Also, the larger components of the joined modes coincide with most powerful separate modes, compare: top(a)$\approx$top(f), bottom(b)$\approx$bottom(f), top(c)$\approx$bottom(g), bottom(d)$\approx$-bottom(g). These are indications of statistical independence of the two signals.

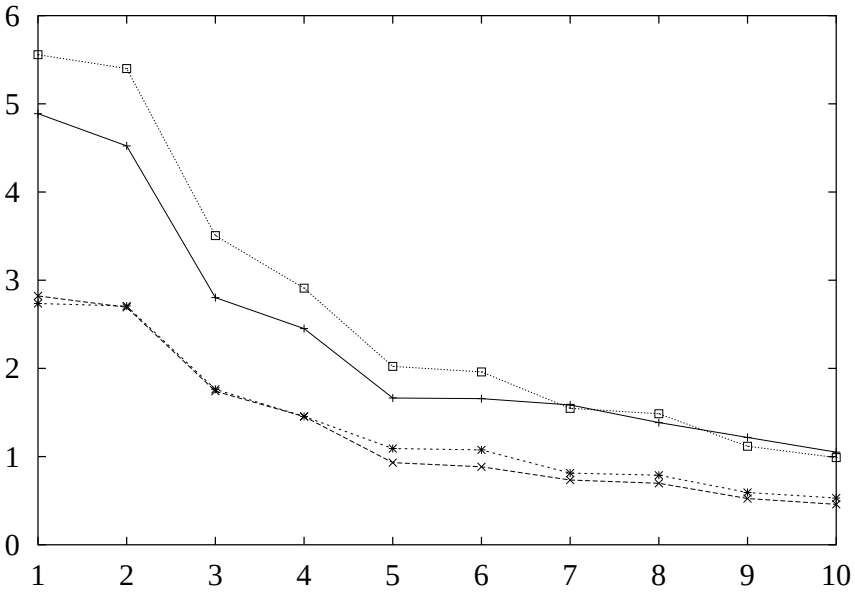

FIGURE 11. KL spectra of the surface patterns of the numerical simulations of Figure 1: amplitudes of eigenfunctions vs their ordinal number. Format the same as in Figure 6.

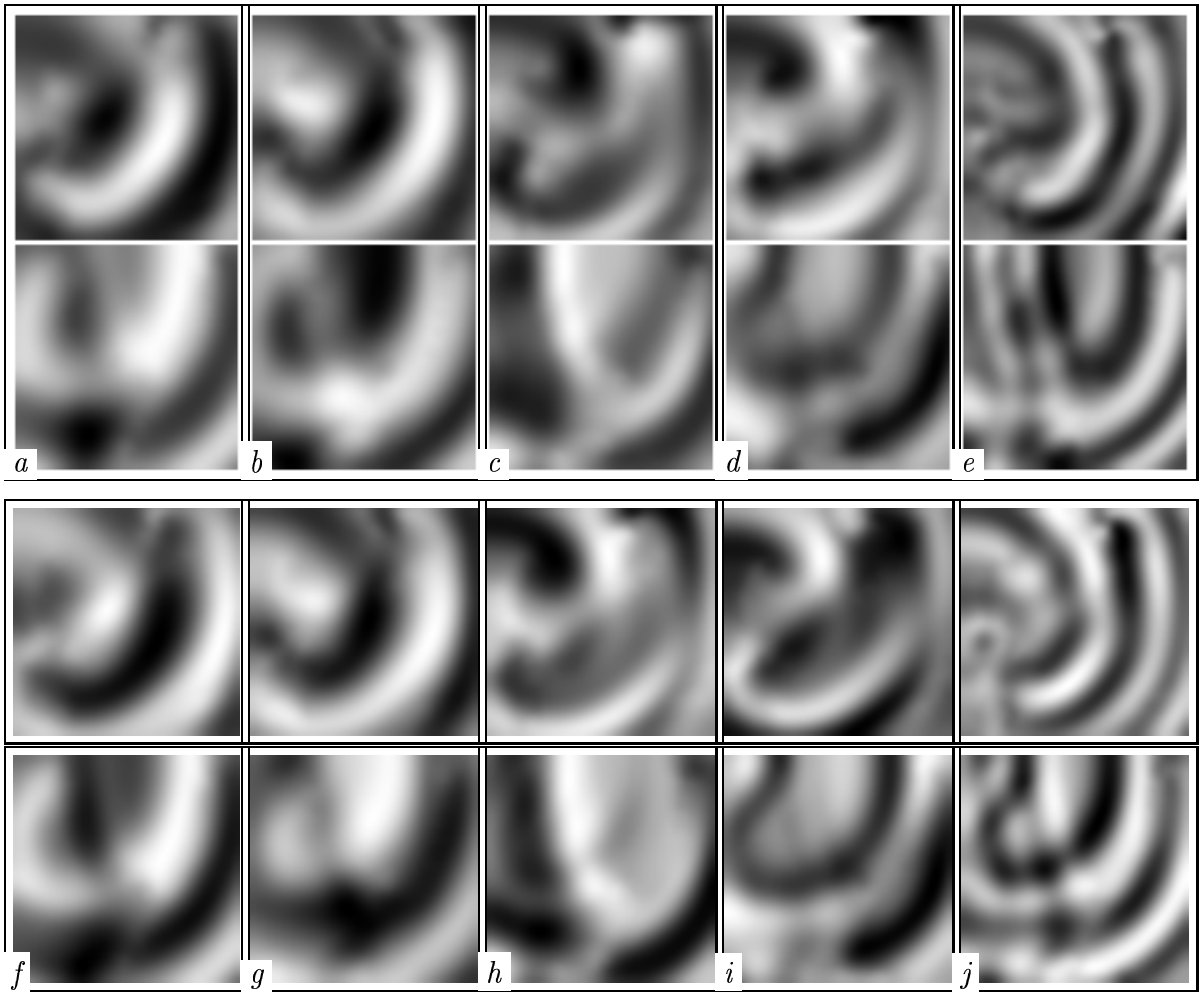

FIGURE 12. The principal KL modes of the surface patterns from the numeric scroll turbulence of Figure 1. Format the same as in Figure 7.

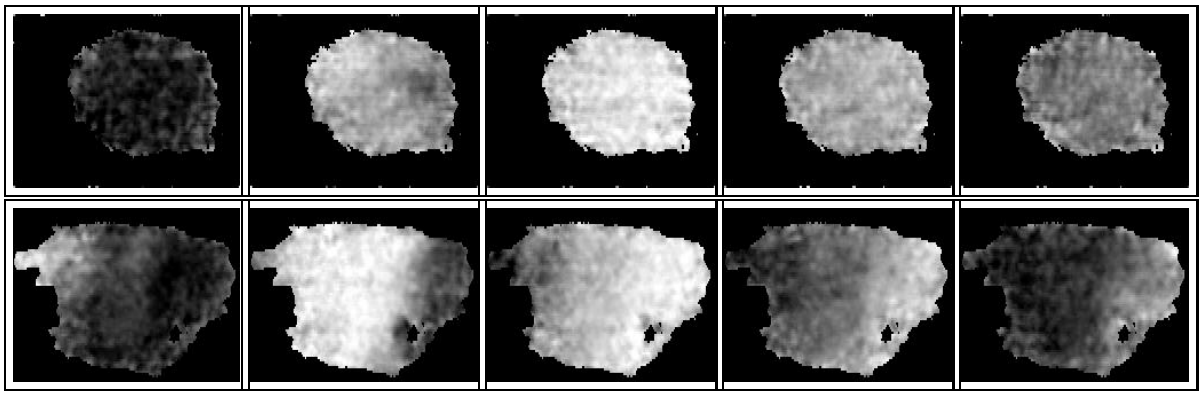

FIGURE 13. Surface activity during a polymorphic tachycardia, epicardial surface above, endocardial surface below. Each pair of images is 33 ms apart, and white areas code the onset of excitation, dark areas recovery from excitation

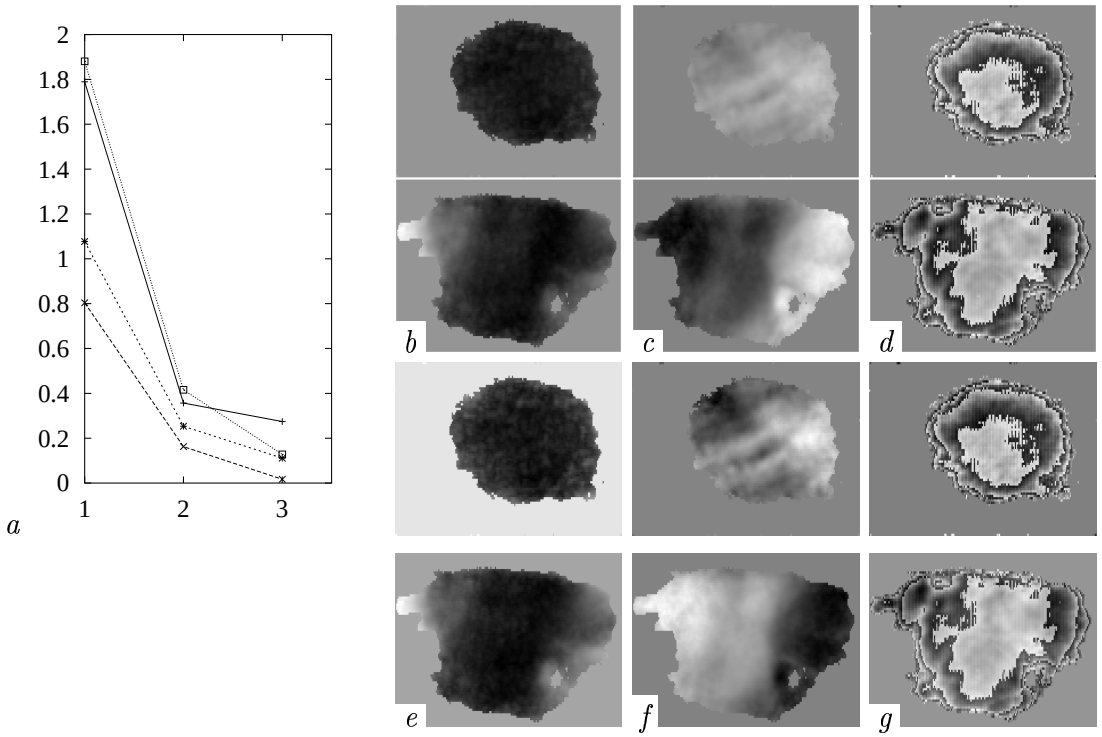

FIGURE 14. (a) The KL spectra and (b–g) the principal KL modes of the experimental monomorphic tachycardia shown on Figure 13: (b–d) processed together, (e–g) separately. Top rows: epicardial surface, bottom rows: endocardial surface.

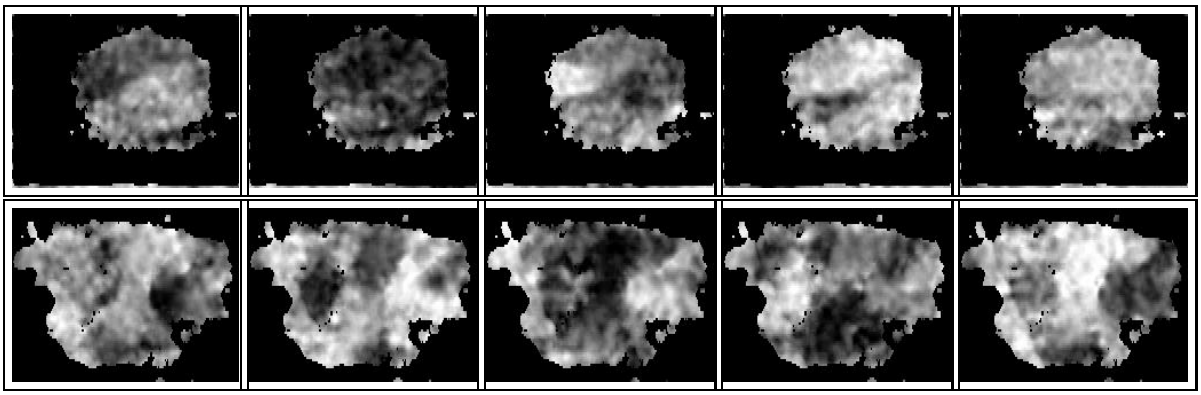

FIGURE 15. Surface activity during a polymorphic tachycardia, epicardial surface above, endocardial surface below . Each pair of images is 33 ms apart, and white areas code the onset of excitation, dark areas recovery from excitation

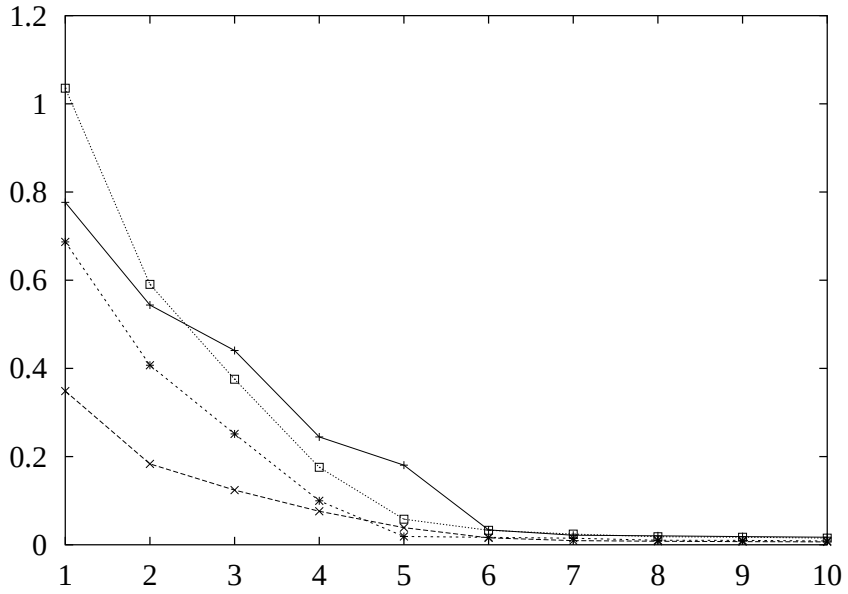

FIGURE 16. KL spectra of the polymorphic tachycardia of Figure 15. Format is the same as in Figure 6.

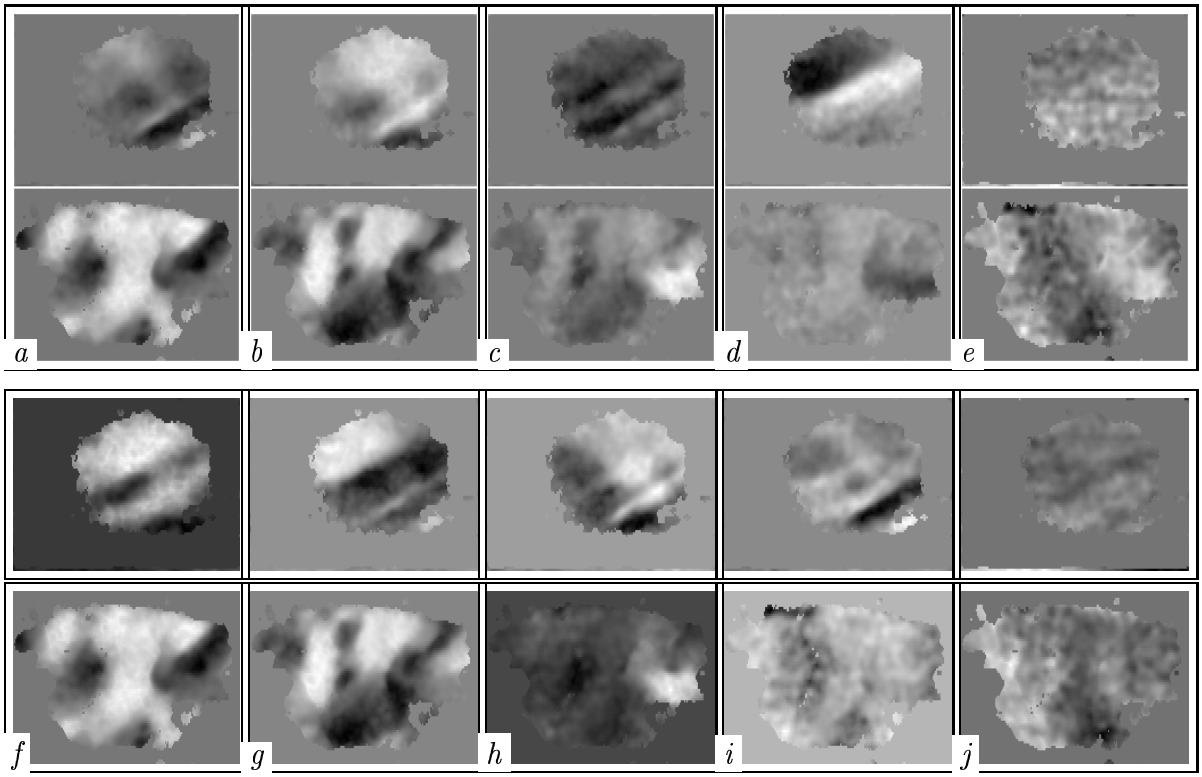

FIGURE 17. The principal KL modes of the experimental polymorphic tachycardia shown on Figure 15. Format the same as in Figure 7.

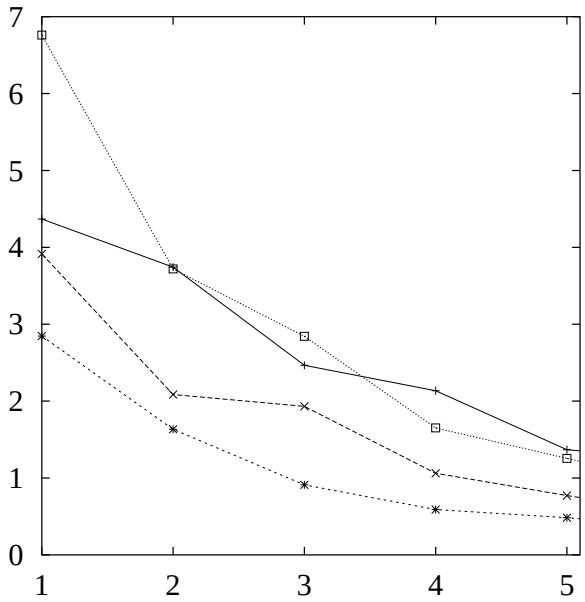

FIGURE 18. KL spectra of the polymorphic tachycardia of Figure 2. Format is the same as in Figure 6.

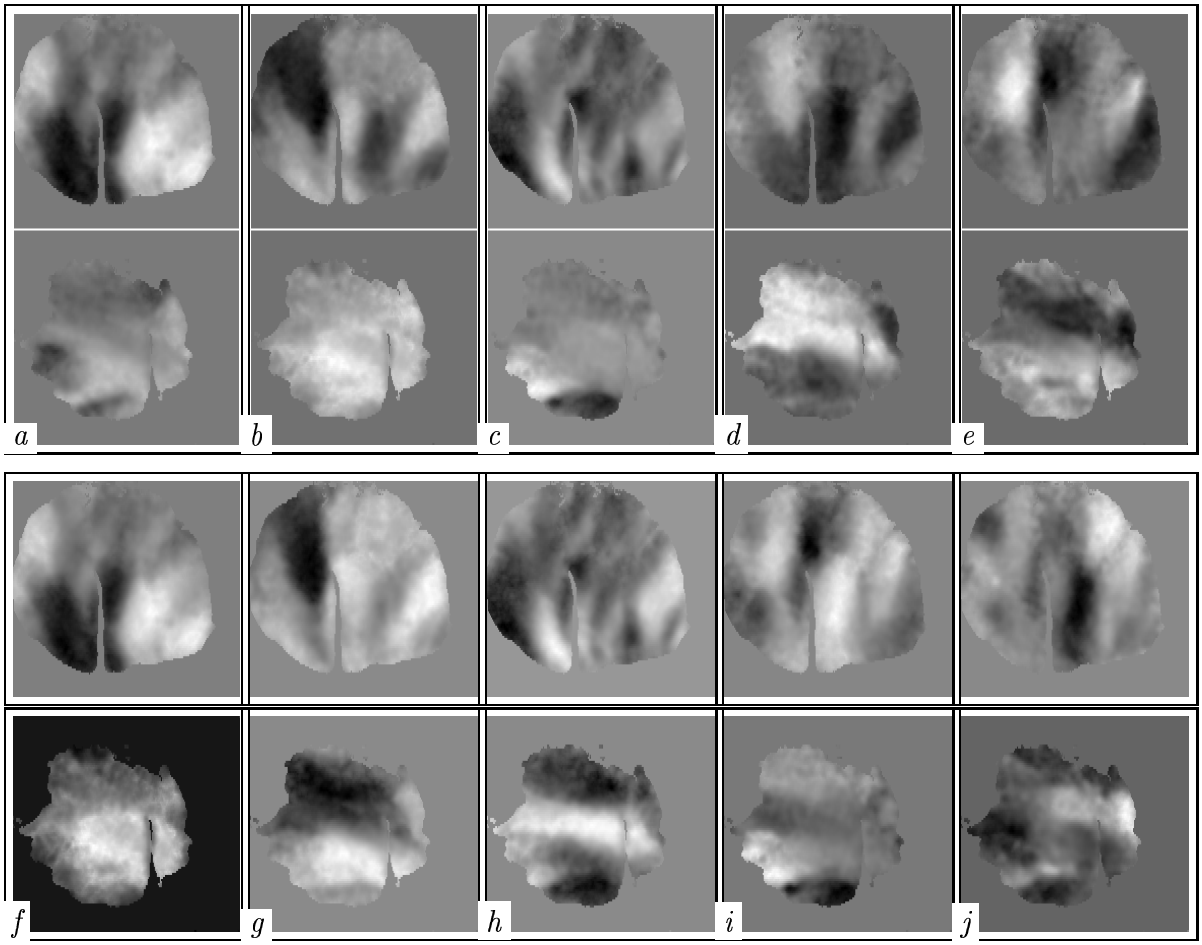

FIGURE 19. The principal KL modes of the polymorphic tachycardia of Figure 2. Format the same as in Figure 7.

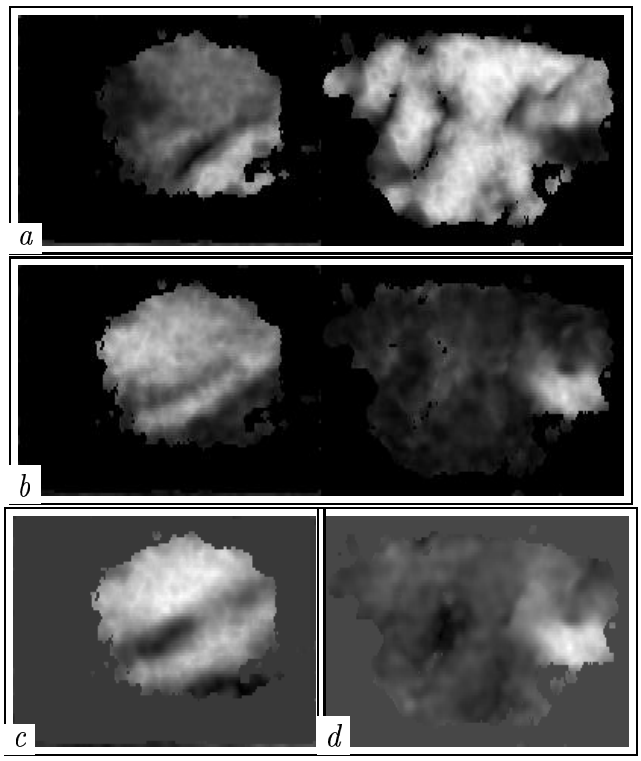

FIGURE 20. Comparison of the frequency domains and selected KL modes of the polymorphic tachycardia of Figure 15. (*a*) The frequency domain corresponding to the higher frequency band, 7.9 Hz. (*b*) The frequency domain corresponding to the lower frequency band, 6.1 Hz. (*c*) The first KL mode of the separate epicardial sequence. (*d*) The third KL mode of the separate endocardial sequence. The two frequency domains are supplements of each other, *i.e.* each point of the preparation, if oscillates, has one of the two frequencies. The selected KL modes are close to the corresponding components of the lower-band domain.